SSRG International Journal of Electrical and Electronics Engineering
ISSN: 2348-8379/ https://doi.org/10.14445/23488379/IJEEE-V12I5P110

Volume 12 Issue 5, 103-115, May 2025
© 2025 Seventh Sense Research Group®

Original Article

A Sliding-PID-Fuzzy Control Strategy with High-Gain Observer for Axial Flux Permanent Magnet Motor Operation

Manh Tung Ngo[1], Van Hung Pham[2], Yen Vu Thi[3]

[1,2,3]*Faculty of Automation Engineering, School of electrical and electronic engineering, Hanoi University of Industry,Vietnam.*

[1]*Corresponding Author : tung_nm@haui.edu.vn*

Received: 05 March 2025 Revised: 10 April 2025 Accepted: 24 April 2025 Published: 31 May 2025

Abstract - *The article details the design of a Sliding-PID-Fuzzy controller with a high-gain observer for the drive system of an axially-gapped permanent magnet motor. This motor integrated a magnetic bearing, torque, and axial force generated by the interaction of the stator magnetic field with the permanent magnet field of the rotor. Based on the dynamic state equations of the motor, the Sliding-PID-Fuzzy controller helps stabilize the rotor position and control the speed. Concurrently, the developed controller incorporates fuzzy logic techniques to effectively mitigate the classical chattering phenomenon caused by the control signal. The High-gain observer is applied to observe the system's disturbance and pre-estimate uncertain components. Simulation results demonstrate that the control system exhibits strong stability, reduced steady-state error, and enhanced robustness.*

Keywords - *Fuzzy, SMC, Chattering, High-gain observer, Axial flux motor, Axial gap motor.*

1. Introduction

The Axial Flux Permanent Magnet Motor (AFPMM) is a high-tech product used to replace conventional bearing motors in certain specialized fields. The major difference from conventional bearing motors is that the AFPMM employs magnetic force to lift the motor shaft and eliminate physical contact. This operation at high speeds ensures good operational quality even in harsh environments, reducing maintenance costs [1]-[4]. Axial Flux Permanent Magnet Motor system typically consists of two control systems: the first control system generates lifting force vertically perpendicular to the motor shaft, while the second control system regulates rotational motion and fixes the axial displacement of the motor shaft [5]-[7].

The control structure of the transverse AFPMM has been addressed in various studies [2],[4],[10]-[13]. However, this paper focuses solely on the design of the control system corresponding to the second control system mentioned above. Figure 1 illustrates the structure of the AFPMM. In this configuration, two transverse axis reluctances generate a lifting force horizontally. The axial force along the shaft stabilizes the rotor's axial position while also producing rotational torque. The rotation of this motor is achieved through the interaction between the stator's rotating magnetic field and the rotor's permanent magnet field, generating the necessary torque.

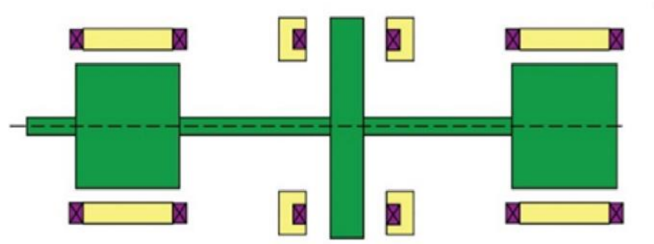

Fig. 1 The structure of the Axial Air Gap Magnetic Bearing Motor

Numerous studies have presented control strategies based on the vector control principle [14]-[21], with the axial force regulated by the d-axis current component and the electromagnetic torque managed by the q-axis current component [14]. In papers such as [6], [8], and [16]-[18], linear PID controllers are used, making system performance extremely dependent on model correctness and sensitive to external disturbances. Alternatively, sliding mode controllers have been presented in [5], [7], [15], and [21] to improve system resilience against uncertainties; however, these designs focus exclusively on speed control and are generally used with traditional PMSMs. Using sliding mode approaches, nonlinear controllers are devised in [11] and [19] for PMSM speed and axial position adjustment. However, these methods still suffer from chattering effects during operationulation of PMSMs utilizing sliding mode techniques and steady-state errors under disturbance since they rely on reduced mathematical models.

With the relatively limited research on this type of AFPMM compared to traditional bearing motors, this paper employs simplified mathematical models for control system design. However, this simplification may lead to operational inaccuracies and instability when uncertain disturbances occur. Thus, a combination of observer-based disturbance estimation and robust control strategies is necessary for effective motor operation. This paper focuses on designing a High-gain disturbance observer to estimate uncertain disturbances caused by parameter variations in the motor. Additionally, a PID sliding mode controller combined with a Fuzzy controller (SMC-PID-Fuzzy) is utilized to eliminate chattering entirely [9,10]. The control system consists of two controllers to stabilize rotor position while simultaneously responding to motor speed changes. Therefore, the proposed observer is crucial for observing system disturbances accurately. The effectiveness of the proposed control systems is demonstrated through simulation using MATLAB-Simulink software.

2. Mathematical Model of the Motor

The research engine comprises a rotor and two stators. The engine's structure [6],[7],[18] is depicted in Figure 2. It is assumed that the parameters along the x, y, Ѳx, and Ѳy axes of the rotor are controlled by controlling the horizontal axis electromagnets. The paper focuses solely on designing corresponding sliding mode controllers for the two degrees of freedom: the longitudinal position and the rotational speed of the rotor. Following the principle of field-oriented control, the quantities and parameters of the motor are transformed into the dq rotating coordinate system through coordinate transformation matrices (Hedrick) [13]. The mathematical model of the research engine contains some uncertain components due to the stator's self-inductance being inversely proportional to the air gap g according to the following approximate formula [8], [21]:

$$L_{sd} = \frac{3}{2}\frac{L'_{sd0}}{g} + L_{sl} \quad (1)$$

$$L_{sd} = \frac{3}{2}\frac{L'_{sd0}}{g} + L_{sl} \quad (2)$$

L'_{sd0} and L'_{sq0} are the synchronous inductances along the d-axis and q-axis per unit length; L_{sl} is the leakage inductance. $g = g_0 \pm z$ represents the air gap between the rotor and stator; g_0 is the air gap at the equilibrium position; z is the displacement from the equilibrium position.

The mathematical model of the synchronous research engine is represented on the rotating coordinate system d,q as follows [7]:

$$\begin{cases} u_{sd} = R_s i_{sd} + L_{sd} d_{i_{sd}}/dt - \omega_e L_{sq} i_{sq} \\ u_{sq} = R_s i_{sq} + L_{sq} d_{i_{sq}}/dt + \omega_e L_{sd} i_{sd} + \omega_e \lambda_m \\ \lambda_{sd} = L_{sd} i_{sd} + \lambda_m \\ \lambda_{sq} = L_{sq} i_{sq} \end{cases} \quad (3)$$

With λ_m being the flux linkage due to the magnetic field generated by the rotor on the stator, i_{sd} and i_{sq} are the stator current components; u_{sd} and u_{sq} are the stator voltage components; ω is the rotor speed; λ_{sd} and λ_{sq} are the stator flux linkages. According to [7,14,15], the torque is controlled by the *q*-axis current, while the flux is controlled by the *d*-axis current. We have:

$$\begin{cases} i_{q1} = i_{q2} = i_q \\ i_{d1} = i_{d0} - i_d \\ i_{d2} = i_{d0} + i_d \end{cases} \quad (4)$$

Where: i_{d1} and i_{d2} are the *d*-axis currents of the two stators; i_{d0} is the negligible or zero compensating current. The axial force and total torque exerted on the rotor by the two stators [3]:

$$F = 4K_{Fd}(i_f + i_{d0})i_d$$
$$+4\left[K_{Fd}(i_d^2 + i_{d0}^2 + i_f^2) + 2K_{Fd} i_f i_{d0} + K_{Fq} i_q^2\right]\frac{z}{g_0} \quad (5)$$

$$T = 2K_T i_q + 2K_R i_q i_{d0} + \frac{2K_R i_d i_q z}{g_0} \quad (6)$$

With i_f being the DC current converted from the permanent magnet field of the rotor.

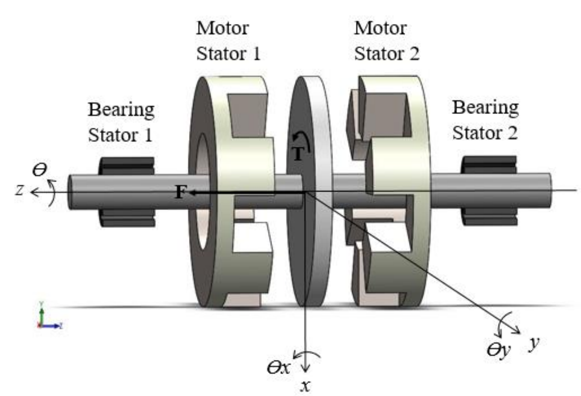

Fig. 2 The structure of the Axial Air Gap Magnetic Bearing Motor

Although the axial force F still has a small dependence on the *q*-axis current component and the torque T still has a small dependence on the *d*-axis current component, the characteristic signals for controlling force F by current i_d and torque T by current i_q. We have the dynamic characteristic equation of the motor's axial position as follows:

$$\ddot{z} = \frac{F - F_L}{m} = \frac{4K_{Fd} i_f i_d}{m} +$$

$$\frac{4K_{Fd}i_{d0}i_d+4\left[K_{Fd}\left(i_d^2+i_{d0}^2+i_f^2\right)+2K_{Fd}i_f i_{d0}+K_{Fq}i_q^2\right]\frac{z}{g_0}}{m} - \frac{F_L}{m} \quad (7)$$

The dynamic equation of motor speed:

$$\dot{\omega} = \frac{T-T_L}{J} = \frac{2K_T i_q}{J} + \frac{2K_R i_q i_{d0} + \frac{2K_R i_d i_q z}{g_0}}{J} - \frac{T_L}{J} \quad (8)$$

Where F_L and T_L respectively represent the axial load disturbance and the torque load disturbance. We set the corresponding parameters as follows:

$$d_z = \frac{4K_{Fd}i_{d0}i_d+4\left[K_{Fd}\left(i_d^2+i_{d0}^2+i_f^2\right)+2K_{Fd}i_f i_{d0}+K_{Fq}i_q^2\right]\frac{z}{g_0}}{m} \quad (9)$$

$$d_\omega = \frac{2K_R i_q i_{d0} + \frac{2K_R i_d i_q z}{g_0}}{J} \quad (10)$$

The parameters d_z and $d\omega$ are the components causing cross-coupling effects between equations (11) and (12). These parameters d_z and $d\omega$ can be considered as uncertain components of the system.

Therefore, we can define d_1 and d_2 as the system disturbances comprising load disturbances and uncertain components as follows:

$$d_1 = d_z - \frac{F_L}{m} \quad (11)$$

$$d_2 = d_\omega - \frac{T_L}{J} \quad (12)$$

2.1. Designing a Position Control System Utilizing a PID Sliding mode Controller Combined with a Fuzzy Controller:

Sliding mode control is a nonlinear control method applied to the following system. Considering $x \in R^n$ as the state vector, u as the control signal, $s=s(t,x)$ as the sliding surface, we have the following system:

$$\ddot{x}(t) = f(t,x,u) \quad (13)$$

$$s = s(t,x) \quad (14)$$

To minimize the chattering phenomenon, we add an additional control current from the output of the fuzzy controller, as shown in the control system structure in Figure 3.

In that case, the position control signal is obtained as follows: $i_d = i_{dz} + i_{Fz}$

The axial error is calculated as follows:

$$m\ddot{z} = F - F_L \quad (15)$$

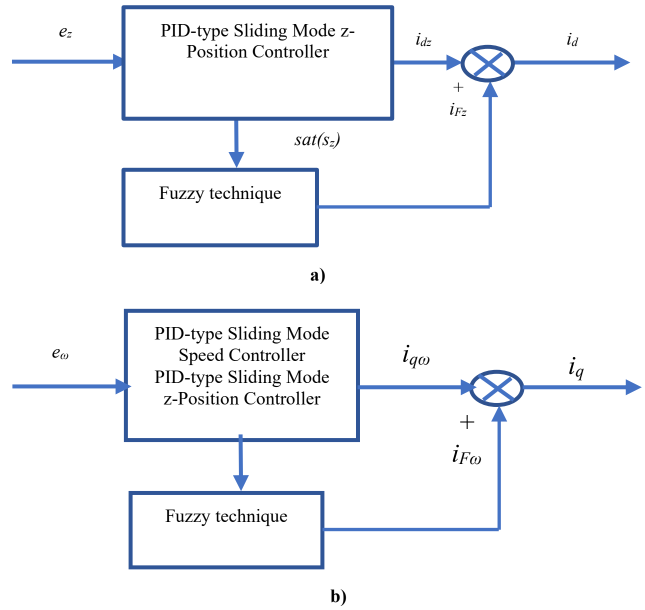

Fig. 3 Block Diagram of the Sliding-PID-Fuzzy Controller for a) Axial Position Control and b) Motor Speed Control.

With m being the mass of the moving part, F being the axial attractive force, and F_L being the axial load force. From equation (7), we have:

$$\ddot{z} = 4K_{Fd}i_f i_d/m + d_1 \quad (16)$$

Let's assume the desired position is z_{Ref}. Then, we have:

$$e_{1z} = z_{Ref} - z \quad (17)$$

$$e_{2z} = \dot{z}_{Ref} - \dot{z} \quad (18)$$

The error of the system is defined as:

$$\dot{e}_{1z} = e_{2z}\ \dot{e}_{2z} = \ddot{z}_{Ref} - \frac{4K_{Fd}i_f i_d}{m} - d_1 \quad (19)$$

Selecting the sliding surface as:

$$s_1(t) = \dot{e}_{1z}(t) + \lambda_1 e_{1z}(t) + \lambda_2 \int_0^t e_{1z}(\tau)d(\tau)$$

$$\dot{s}_1(t) = \ddot{e}_{1z}(t) + \lambda_1 \dot{e}_{1z}(t) + \lambda_2 e_{1z}(t)$$

$$= \ddot{z}_{Ref} - \frac{4K_{Fd}i_f i_d}{m} - d_1 + \lambda_1 \dot{e}_{1z}(t) + \lambda_2 e_{1z}(t) \quad (20)$$

With λ_1 and λ_2 being positive constants and the controller needing to drive $s_1(t)$ to 0, choose a positive definite Lyapunov function V_1:

$$V_1(s) = s_1^2/2 \quad (21)$$

According to the Lyapunov stability criterion, for the system to be asymptotically stable, we need $\dot{V}_1 < 0$. Therefore, we choose the output current signal:

$$i_{dz} = \frac{m}{4K_{Fd}i_f}[\ddot{z}_{Ref} - d_1 + \lambda_1(\dot{z}_{Ref} - \dot{z}) +$$
$$+\lambda_2(z_{Ref} - z) + k_z sat(s_1) + \eta_z s_1] \tag{22}$$

With k_z, η_z being pre-selected positive constants.
Therefore, $\dot{s}(t) = -k_z sat(s_1(t)) - \eta_z s_1(t)$

When $s_1(t) < 0$, $\dot{V}_1 = s_1.\dot{s}_1 = -s_1[k_z sat(s_1(t)) + \eta_z s_1(t)] < 0$

When $s_1(t) > 0$, $\dot{V}_1 = s_1.\dot{s}_1 = -s_1[k_z sat(s_1(t)) + \eta_z s_1(t)] < 0$

The signal $sat(s_1(t))$ is fed into the Fuzzy controller to control the oscillations of the $sat(s_1)$ function. In Figure 4, NB represents large negative, NM represents medium negative, ZO represents 0, PB represents large positive, and PM represents medium positive.

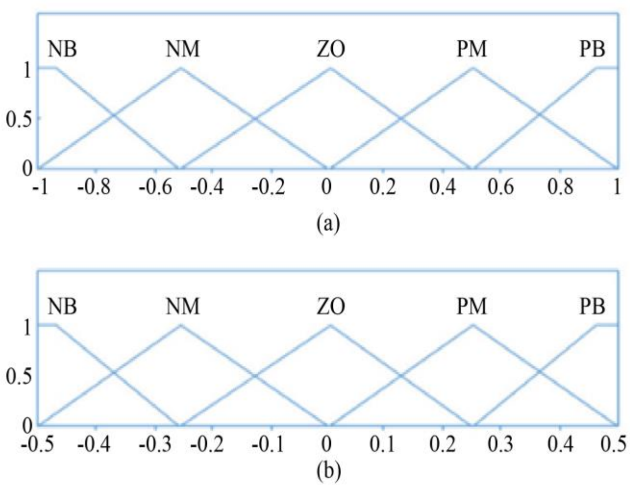

Fig. 4 (a) Fuzzification of the input signal *sat(s_1)* and (b) Fuzzification of the output i_{F1}

Based on the oscillations of the signal of the $sat(s_1)$ function before the Fuzzy controller is applied, the control rules are used as follows:

- If $sat(s_1)$ is NB or $sat(s_1)$ is PM, Then i_{Fz} is PB
- If $sat(s_1)$ is NM or $sat(s_1)$is PB or $sat(s_1)$ is ZO, Then i_{Fz} is PM
- If $sat(s_1)$ is ZO or $sat(s_1)$ is NM or $sat(s_1)$ is PM, Then i_{Fz} is ZO
- If $sat(s_1)$ is PM or $sat(s_1)$ is ZO or $sat(s_1)$ is NB, Then i_{Fz} is NM
- If $sat(s_1)$ is NM or $sat(s_1)$ is PB, Then i_{Fz} is NB

2.2. Designing the Motor Speed Controller

The rotational dynamics of the motor dictate that the difference between the electromagnetic torque T and the load torque T_L produces a net torque, which causes angular acceleration. The rotational motion function of the motor is written as follows:

$$J\dot{\omega} = T - T_L \tag{23}$$

From (8), we have:

$$\dot{\omega} = \frac{T}{J} - \frac{T_L}{J} = \frac{2K_T i_q}{J} + d_2 \tag{24}$$

Let's assume the desired speed is ω_{Ref}

$$e_\omega = \omega_{Ref} - \omega \tag{25}$$

Let's choose the sliding surface as follows:

$$s_2(t) = \dot{e}_\omega(t) + \lambda_3 e_\omega(t) + \lambda_4 \int_0^t e_\omega(\tau)d(\tau)$$
$$\dot{s}_2(t) = \ddot{e}_\omega(t) + \lambda_3\dot{e}_\omega(t) + \lambda_4 e_\omega(t) \tag{26}$$
$$= \ddot{e}_\omega(t) + \lambda_3(\dot{\omega}_{Ref} - \frac{2K_T i_q}{J} - d_2) + \lambda_4 e_\omega(t)$$

With λ_3 and λ_4 being positive constants and the controller needing to drive $s_2(t)$ to 0, let's choose a positive definite Lyapunov function V_2:

$$V_2(s) = s_2^2/2 \tag{27}$$

According to the Lyapunov stability criterion, for the system to be asymptotically stable, we need $\dot{V}_2 < 0$. Therefore, we choose the output current signal:

$$i_{q\omega} = \frac{J}{2K_T}[\frac{k_\omega sat(s_2(t) + \eta_\omega + \ddot{\omega}_{Ref} - \ddot{\omega}}{\lambda_3} - d_2$$
$$+\dot{\omega}_{Ref} + \frac{\lambda_4(\dot{\omega}_{Ref} - \omega)}{\lambda_3}] \tag{28}$$

With k_ω, η_ω being pre-selected positive constants.

Therefore, we get:$\dot{s}_2(t) = -k_\omega sat(s_2(t)) - \eta_\omega s_2(t)$

When $s_2(t) < 0$, $\dot{V}_2 = -s_2[k_\omega sat(s_2(t)) + \eta_\omega s_2(t)] < 0$

When $s_2(t) > 0$, $\dot{V}_2 = -s_2[k_\omega sat(s_2(t)) + \eta_\omega s_2(t)] < 0$

The signal $sat(s_2(t))$ is fed into the Fuzzy controller to control the oscillations of the $sat(s_2)$.

In Figure 5, NB represents large negative, NM represents medium negative, ZO represents zero, PB represents large positive, and PM represents medium positive.

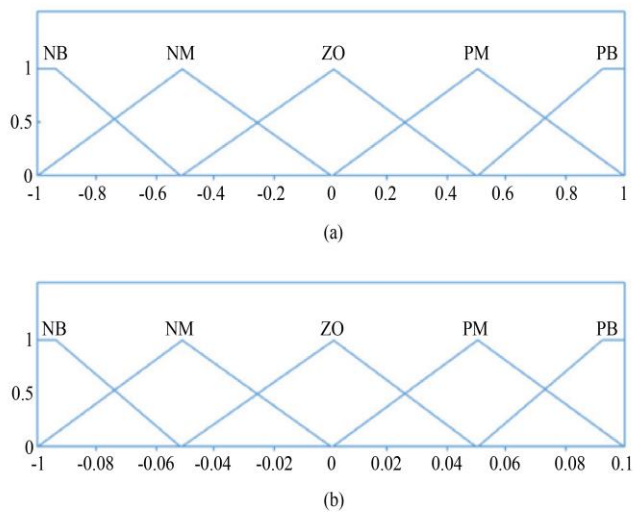

Fig. 5 (a) Fuzzification of the input signal *sat(s_2)* and (b) Fuzzification of the output i_{F2}

Based on the oscillations of the signal of the *sat(s_2)* function before the Fuzzy controller is applied, the control rules are used as follows:

- If *sat(s_2)* is NB or *sat(s_2)* is PM, Then $i_{F\omega}$ is PB
- If *sat(s_2)* is NM or *sat(s_2)* is PB or *sat(s)* is ZO, Then $i_{F\omega}$ is PM
- If *sat(s_2)* is ZO or *sat(s_2)* is NM or *sat(s_2)* is PM, Then $i_{F\omega}$ is ZO
- If *sat(s_2)* is PM or *sat(s_2)* is ZO or *sat(s_2)* is NB, Then $i_{F\omega}$ is NM
- If *sat(s_2)* is NM or *sat(s_2)* is PB, Then $i_{F\omega}$ is NB

To minimize the chattering phenomenon, we add additional control current from the output of the fuzzy controller, and the speed control signal is obtained as follows:

$$i_{control2} = i_{F2} + i_{q\omega}$$

3. Designing a High-Gain Observer for System Disturbance Estimation

Because the system exhibits high nonlinearity during operation, in this case, from the definitions of disturbance d_1 and d_2 in formulas (11) and (12), we can see that these disturbances themselves also contain states of the system (such as the axial position z and the stator current components i_d, i_q. Moreover, the special point of the High-gain observer is that the observation error decreases exponentially and can be applied to nonlinear systems [22]-[24].

Therefore, the objective of this section is to build two High-gain observers to estimate the corresponding disturbance values d_1 and d_2, where d_1 is the system disturbance of the axial position control loop, and d_2 is the system disturbance of the speed control loop [25].

We define the variables as follows:

$$x_1 = z; x_2 = \dot{z}; x_3 = \omega \tag{29}$$

In that case, according to the formulas from equation (7) to equation (10), we have the system of equations as follows:

$$\begin{cases} \dot{x}_1 = x_2 \\ \dot{x}_2 = g_1 i_d + d_1 \end{cases} \tag{30}$$

$$\dot{x}_3 = g_2 i_q + d_2 \tag{31}$$

The estimated errors $\tilde{d}_1$ and $\tilde{d}_2$ of the disturbance d_1 and d_2 are defined as follows:

$$\tilde{d}_i = d_i - \hat{d}_i, i = [1,2] \tag{32}$$

Where $\hat{d}_1$ and $\hat{d}_2$ are the outputs of the disturbance observers. The dynamical characteristic equations of $\hat{d}_1$ and $\hat{d}_2$ in the High-gain observer algorithm are as follows.

$$\dot{\hat{d}}_1 = \frac{1}{\varepsilon_1}\left(\dot{x}_2 - g_1 i_d - \hat{d}_1\right) \tag{33}$$

$$\dot{\hat{d}}_2 = \frac{1}{\varepsilon_2}\left(\dot{x}_3 - g_2 i_q - \hat{d}_2\right) \tag{34}$$

When $1/\varepsilon_1$ and $1/\varepsilon_2$ are the observer gains. According to formulas (33) and (34), the dynamics of $\hat{d}_1$ and $\hat{d}_2$ contain the derivative values of the system state variables x_2 and x_3. The values of state variables x_2 and x_3 are measured by sensors. If the observer gains used have larger values, the measured disturbance will be significantly amplified, causing difficulties in practical implementation [25]. To address this issue, we introduce auxiliary state variables ξ_1 and ξ_2 defined as follows:

$$\xi_1 = \hat{d}_1 - \frac{x_2}{\varepsilon_1}; \xi_2 = \hat{d}_2 - \frac{x_3}{\varepsilon_2} \tag{35}$$

From equations (33) to (35), the system disturbance is estimated by the following equations:

$$\hat{d}_1 = -\frac{x_2 + g_1 i_d}{\varepsilon_1 s + 1} + \frac{x_2}{\varepsilon_1} \tag{36}$$

$$\hat{d}_2 = -\frac{x_3 + g_2 i_q}{\varepsilon_2 s + 1} + \frac{x_3}{\varepsilon_2} \tag{37}$$

We observe that the disturbance observer for load and uncertain components in equations (33) and (34) cannot simultaneously contain derivative terms of state variables x_2 and x_3 while determining $\tilde{d}_1$ and $\tilde{d}_2$. Therefore, using equations (36) and (37) to estimate disturbance instead of equations (33) and (34) will limit the impact of the measured disturbance when increasing the observer gain.

4. Results and Discussion

The basic specifications of the motor are as follows: rotor mass 0.235 kg, moment of inertia 0.000086 kg.m^2; stator resistance 2.6 Ω; magnetizing inductance λ_m = 0.0126 Wb, L'_{sq0} = 9.6 x 10^{-6} Hm, , L'_{sd0} = 8,2 x 10^{-6} Hm, L'_{sl} = 6 x 10^{-3} H, air axial gap g = 1.7 mm. Conducting a simulation of this structure using Matlab-Simulink software yields the following results.

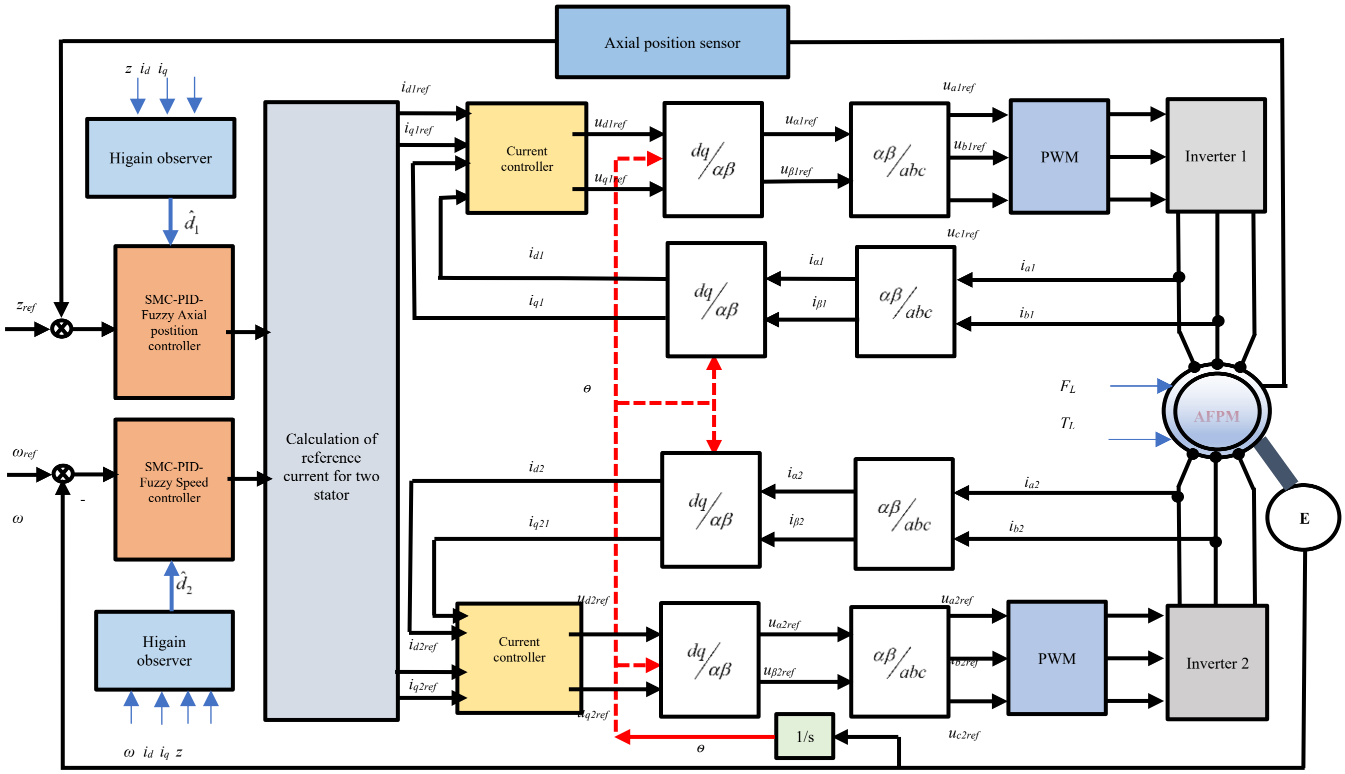

Fig. 6 Design of Control and Observation System

Part 1: Simulation Results of Disturbance Estimation for High-Gain Observer:

When subjected to the effects of F_l = 5N and T_l = 0.1 Nm at 0.2s and 0.4s, respectively. The simulation results are as follows:

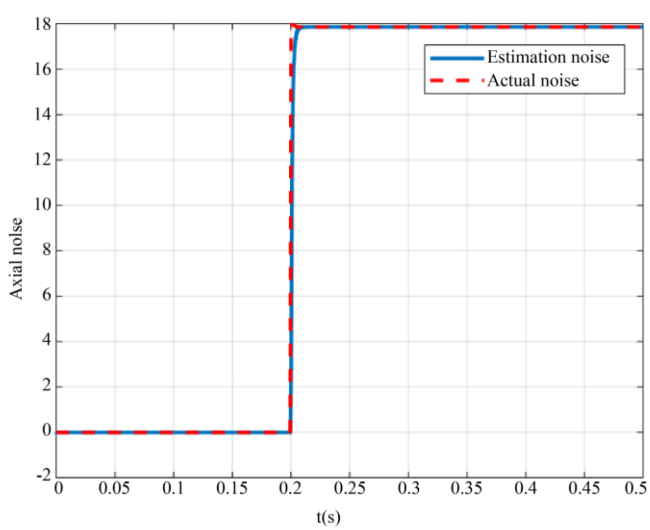

Fig. 7 Axial Load Disturbance Estimation

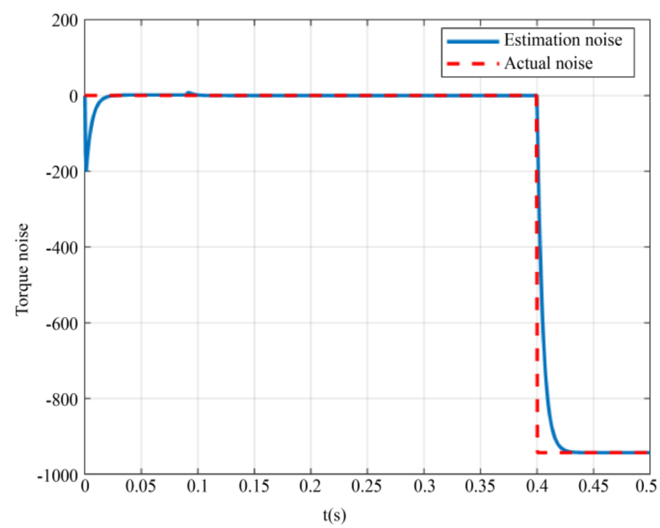

Fig. 8 Moment Load Disturbance Estimation

From both Figures 7 and 8, we observe that the disturbance observer effectively captures both the uncertainty disturbance and the motor load disturbance with good response time. The deviation between the estimated disturbance and the actual disturbance is minimal.

Part 2: Comparison Results of PID-Fuzzy Sliding Controller with PID Sliding Controller.

***Case 1**:* When not subjected to the effects of axial load, F_l and moment T_l.

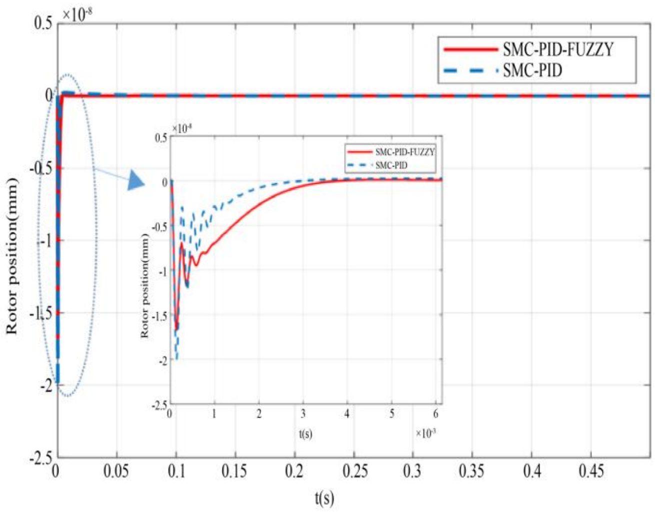

Fig. 9 Rotor Position under no load

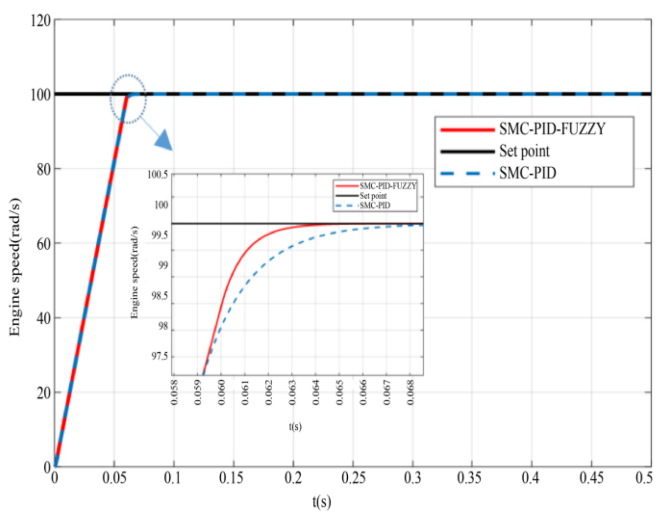

Fig. 10 Motor Speed under no load

Table 1. The comparison results of the quality between the sliding-PID-Fuzzy controller and the sliding-PID controller

		Sliding-PID-Fuzzy	Sliding-PID
Position Response	Settling Time (s)	0.0045	0.006
	Deviation from Setpoint (%)	0	0
Speed Response	Settling Time (s)	0.085	0.09
	Deviation from Setpoint (%)	0	0

From Figures 9 and 10, we observe that when there is no influence of axial load F_l and moment load T_l, the PID-Fuzzy sliding controller exhibits better simulation results in terms of response time compared to the PID sliding controller.

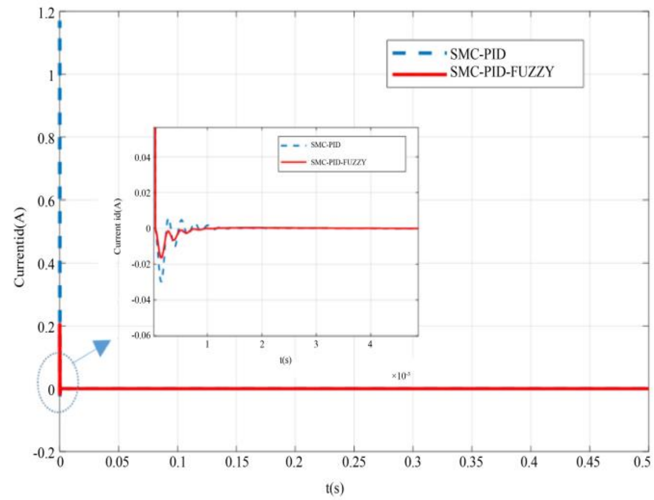

Fig. 11 Current id Response under no load

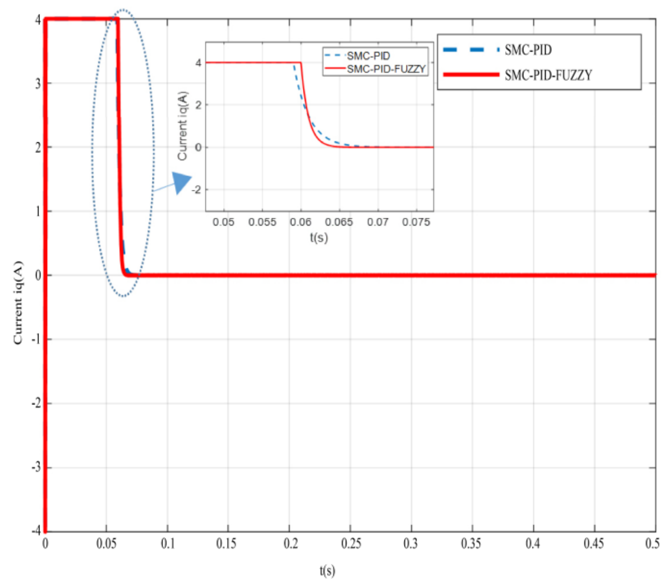

Fig. 12 Current i_q Response under no load

Case 2: When subjected to the effects of axial load F_l = 5N and moment load T_l = 0.1 Nm at time instances 0.2s and 0.4s, respectively.

Figures 13 and 14 demonstrate that the PID-Fuzzy sliding controller performs better in simulation results in terms of overshoot and response time compared to the PID sliding controller.

However, there still exists a speed deviation when subjected to a moment load at 0.4s.

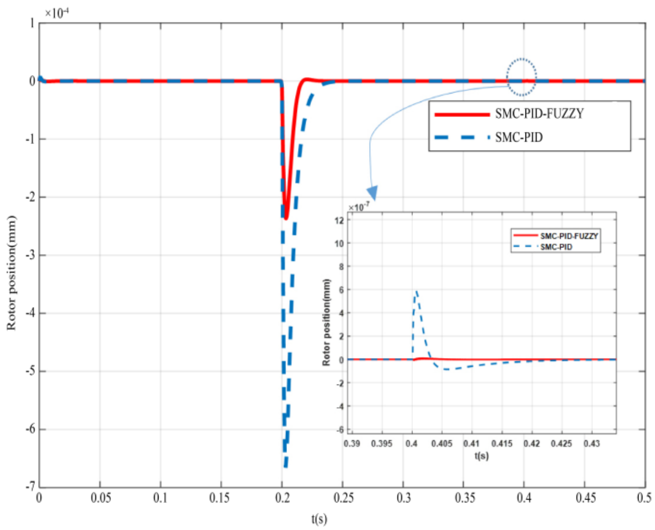

Fig. 13 Rotor Position under load

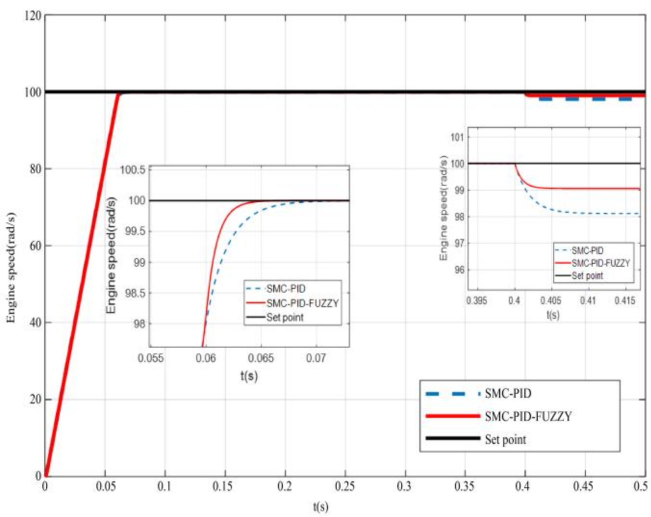

Fig. 14 Motor speed under load

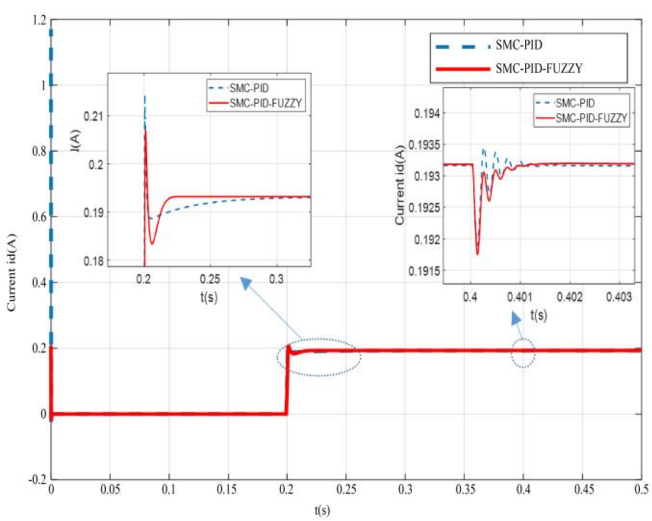

Fig. 15 Current i_d Response under load

Table 2. The comparison results of the quality between the sliding-PID-Fuzzy controller and the sliding-PID controller

		Sliding-PID-Fuzzy	Sliding-PID
Position Response	Settling Time (s)	0.05	0.03
	Deviation from Setpoint (%)	0.003	0.006
Speed Response	Settling Time (s)	0.004	0.010
	Deviation from Setpoint (%)	1	2

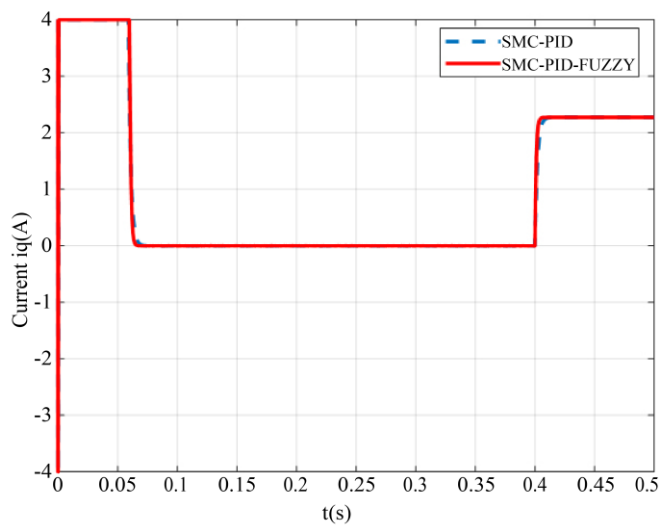

Fig. 16 Current i_q Response under load

Case 3: When the speed is increased from 150 rad/s to 200 rad/s at time 0.6s while still being subjected to the effects of axial load and restraining torque. The results are as follows:

We observe that when the motor speed is changed at time 0.6s, the PID-Fuzzy sliding controller responds faster compared to the PID sliding controller and also has a minor impact on the position.

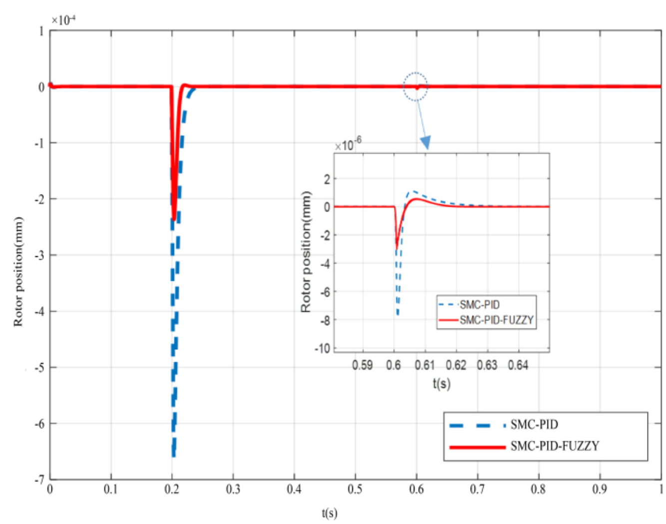

Fig. 17 Rotor Position under speed setpoint change

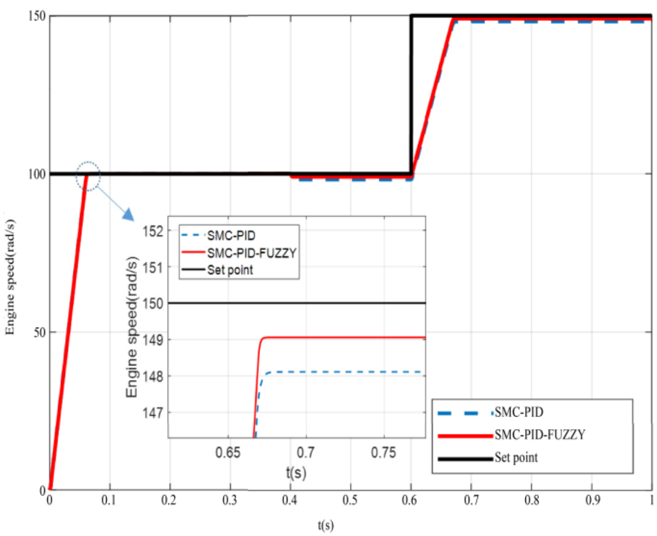

Fig. 18 Motor Speed under speed setpoint change

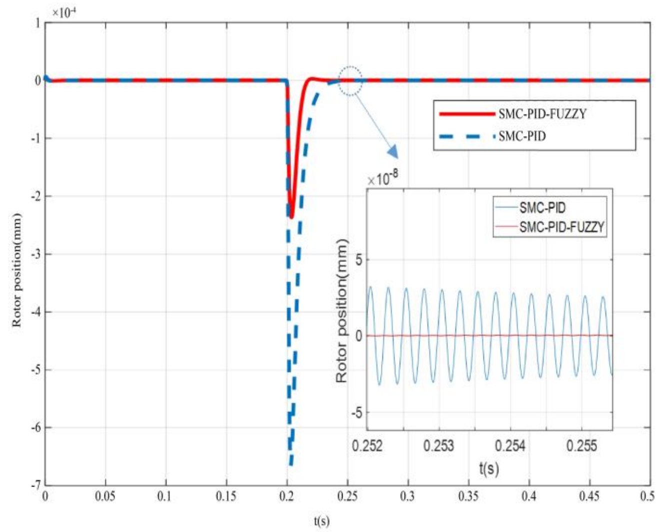

Fig. 21 Chattering Phenomenon Corresponding to Position Response

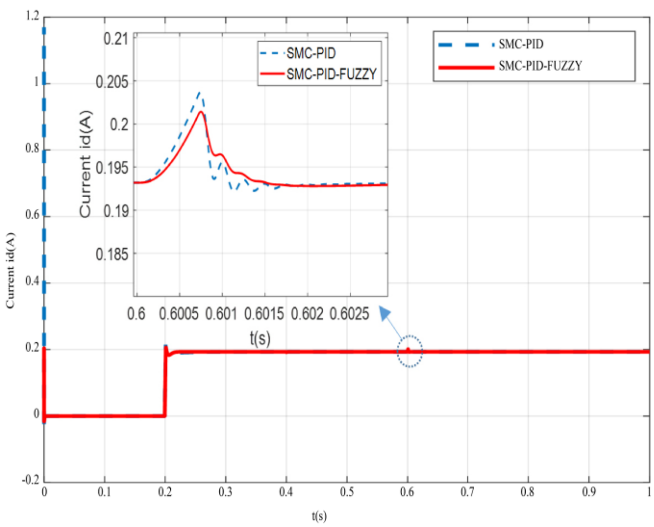

Fig. 19 Current i_d Response under speed setpoint change

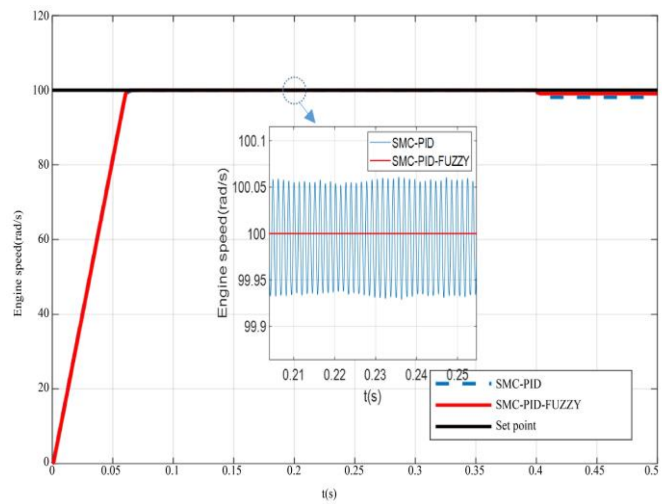

Fig. 22 Chattering Phenomenon Corresponding to Speed Response

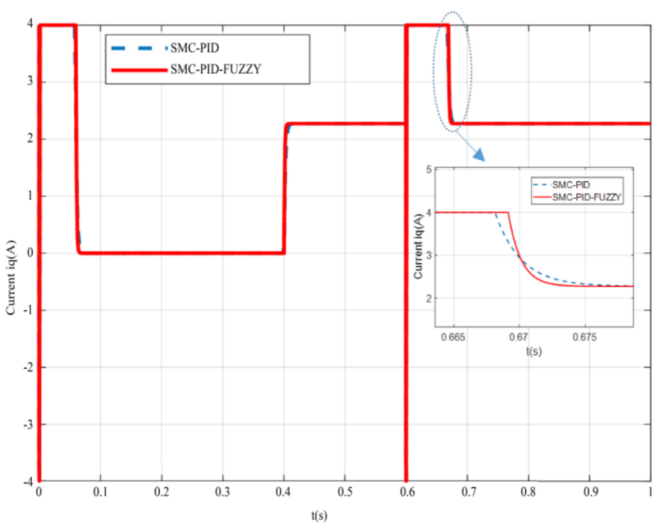

Fig. 20 Current i_q Response under speed setpoint change

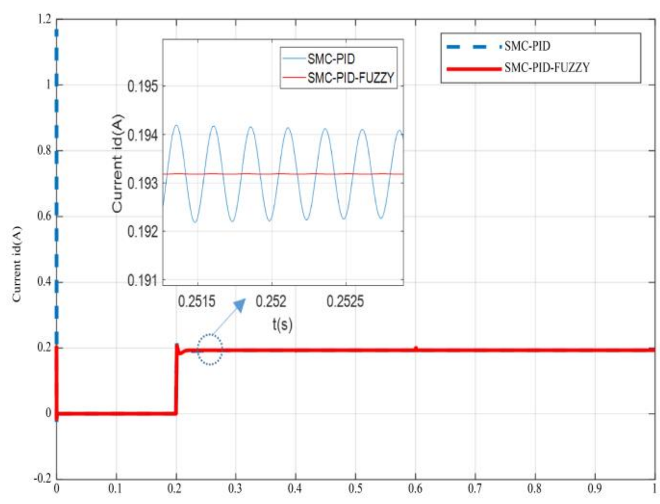

Fig. 23 Current i_d Response

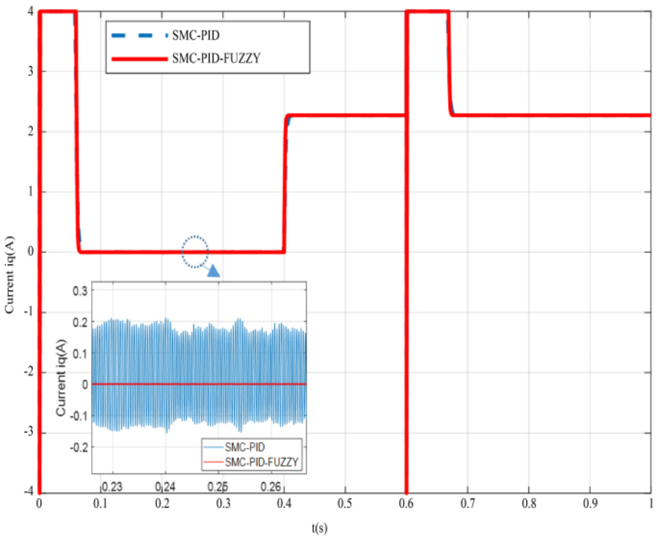

Fig. 24 Current i_q Response

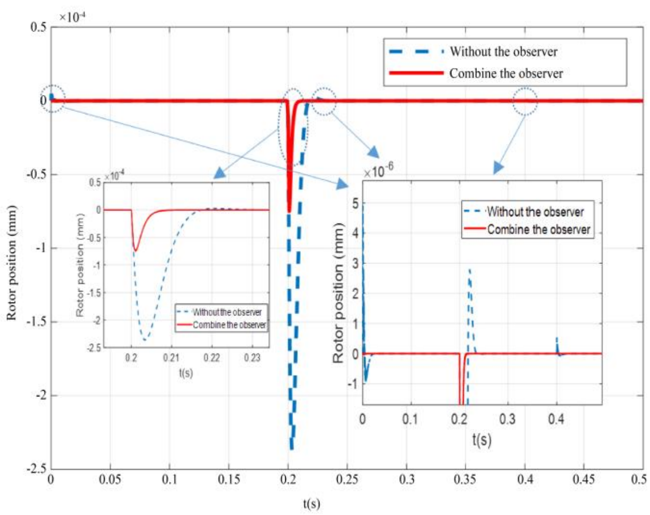

Fig. 25 Rotor Position Response when Combined with Observer

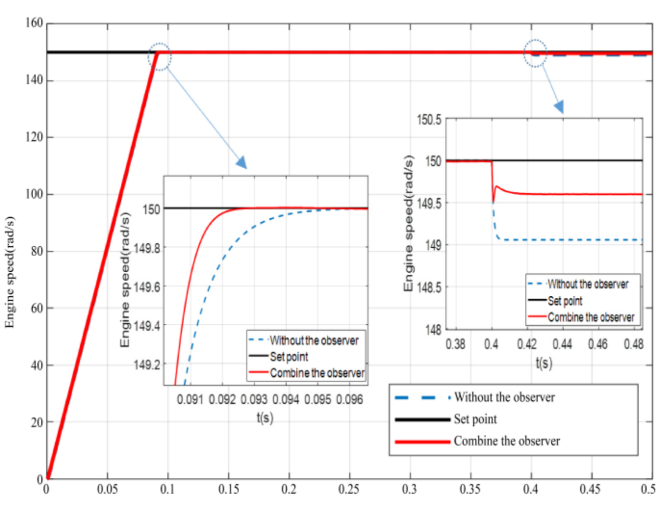

Fig. 26 Motor Speed Response when Combined with Observer

Part 3: Simulation Results of PID-Fuzzy Sliding Controller when Combined with High-Gain Observer

Case 1: When subjected to axial load (F_l = 5N) and moment (T_l = 0.2Nm) at time instances 0.2s and 0.4s, respectively.

In Figures 25 and 26, we observe optimal performance both in terms of speed and rotor position stability when combined with the observer. In the presence of disturbances, the controller, combined with the observer, adapts better and is less affected in terms of settling time and overshoot.

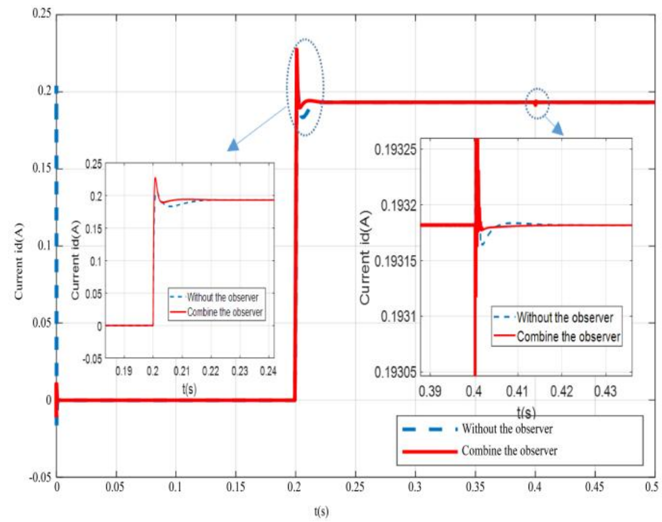

Fig. 27 Current i_d Response when Combined with Observer

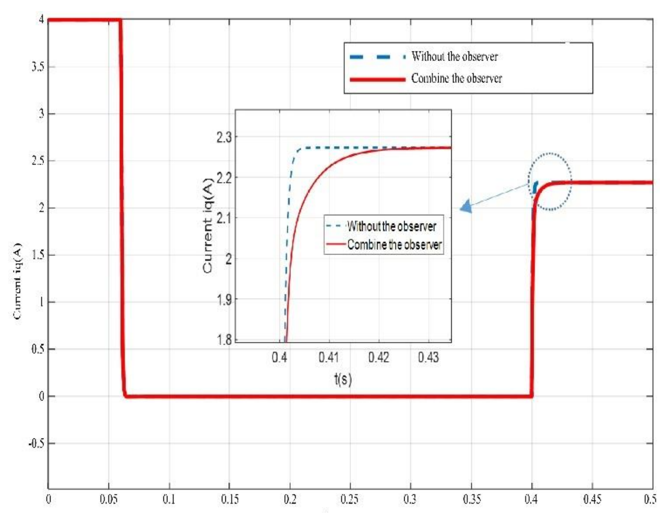

Fig. 28 Current i_q Response when Combined with Observer

Table 3. Simulation Results of PID-Fuzzy Sliding Controller when Combined with High-Gain Observer

		Combined with the observer	Without the observer
Position	Settling Time	0.001	0.003

Response	(s)		
	Overshoot (%)	0	0.003
Speed Response	Settling Time (s)	0.006	0.004
	Overshoot (%)	0.2	1

Case 2: When the speed is increased from 150 rad/s to 200 rad/s at time 0.6s while still being subjected to the effects of axial load and restraining torque. The results are as follows:

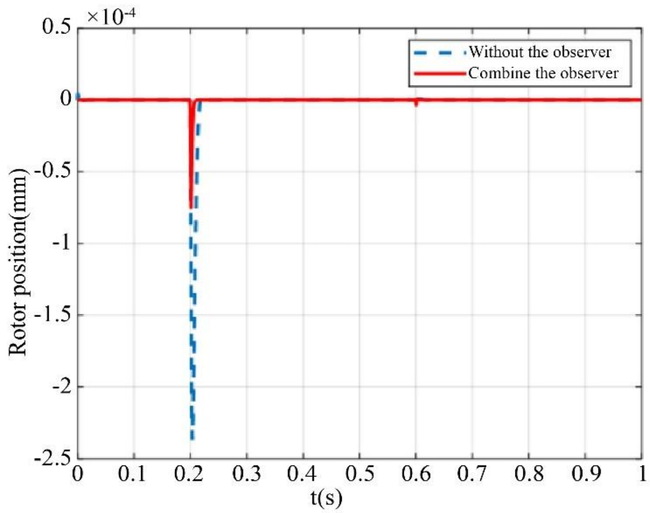

Fig. 29 Rotor Position (with observer) during speed reference Change

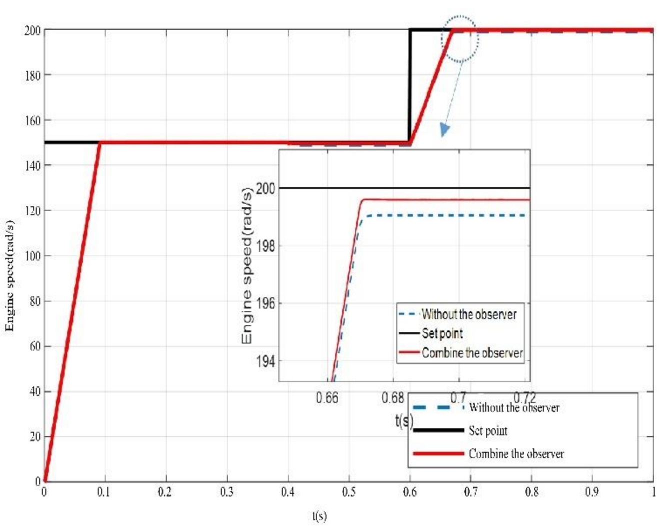

Fig. 30 Motor Speed (with observer) during speed reference Change

We observe that the speed response of the controller combined with the disturbance observer is better, faster, and less deviated compared to the controller without the observer. Additionally, the position controller is not affected by speed changes (Figures 29 and 30).

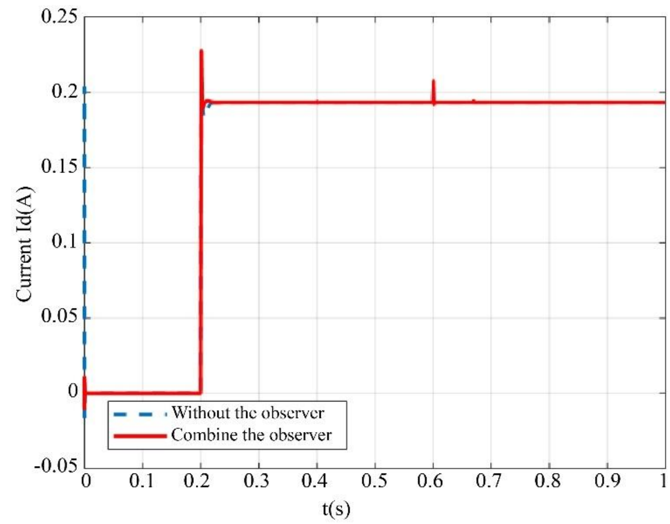

Fig. 31 Current i_d Response (with observer) during speed reference Change

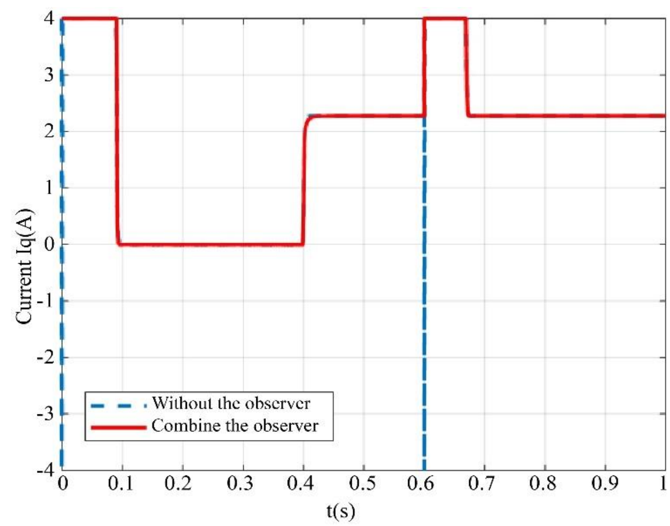

Fig. 32 Current *iq* Response (with observer) during speed reference Change

5. Conclusion

The paper presents a control method employing sliding mode control with PID sliding surface combined with Fuzzy logic and high-gain disturbance observer into the control loop for the vertical position and speed control of a vertical axis thrust air gap motor.

The control signals are designed to be robust against the influence of uncertain components of the motor, which inherently degrade the control response quality.

Simulation results clearly demonstrate the system's high stability and adaptability to load disturbances, significantly outperforming conventional PID sliding mode control systems. Future work could involve developing control strategies for electric vehicle drive systems employing Axial Flux Permanent Magnet Motors.

Funding Statement
We would like to express our gratitude to Hanoi University of Industry for their support in this research within the framework of the scientific research topic under decision number 17-2023-RD/HĐ-ĐHCN.

References
[1] Pekko Jaatinen, "*Design and Control of a Permanent Magnet Bearingless Machine*," Doctoral thesis, Lappeenranta-Lahti University of Technology LUT, 2019. [Google Scholar] [Publisher Link]

[2] Xiaodong Sun, Long Chen, and Zebin Yang, "Overview of Bearingless Induction Motors," *Mathematical Problems in Engineering*, vol. 2014, pp. 1-10, 2014. [CrossRef] [Google Scholar] [Publisher Link]

[3] Satoshi Ueno, and Yoji Okada, "Vector Control of an Induction Type Axial Gap Combined Motor-Bearing," *Transactions of the Japan Society of Mechanical Engineers (C)*, vol. 66, no. 641, pp. 131-137, 2000. [CrossRef] [Google Scholar] [Publisher Link]

[4] B. Lapotre, N. Takorabet, and F. Meibody-Tabarb, "Permanent Magnet Bearingless Motors: Modelling, Design and Drive," *2017 IEEE Workshop on Electrical Machines Design, Control and Diagnosis (WEMDCD)*, Nottingham, UK, pp. 119-126, 2017. [CrossRef] [Google Scholar] [Publisher Link]

[5] Fardila M. Zaihidee, Saad Mekhilef, and Marizan Mubin, "Application of Fractional Order Sliding Mode Control for Speed Control of Permanent Magnet Synchronous Motor," *IEEE Access*, vol. 7, pp. 101765-101774, 2019. [CrossRef] [Google Scholar] [Publisher Link]

[6] Quang Dich Nguyen, and Satoshi Ueno, "Analysis and Control of Nonsalient Permanent Magnet Axial Gap Self-Bearing Motor," *IEEE Transactions on Industrial Electronics*, vol. 58, no. 7, pp. 2644-2652, 2011. [CrossRef] [Google Scholar] [Publisher Link]

[7] Huiming Wang, Shihua Li, and Zhenhua Zhao, "Design and Implementation of Chattering Free Sliding Mode Control Method for PMSM Speed Regulation System," *2015 IEEE International Conference on Industrial Technology (ICIT)*, Seville, Spain, pp. 2069-2074, 2015. [CrossRef] [Google Scholar] [Publisher Link]

[8] Quang-Dich Nguyen, and Satoshi Ueno, *Salient Pole Permanent Magnet Axial-Gap Self-Bearing Motor*, Magnetic Bearings, Theory and Applications, IntechOpen, pp. 61-83, 2010. [Google Scholar] [Publisher Link]

[9] Quang Dich Nguyen, and Satoshi Ueno, "Modeling and Control of Salient-Pole Permanent Magnet Axial-Gap Self-Bearing Motor," *IEEE/ASME Transactions on Mechatronics*, vol. 16, no. 3, pp. 518-526, 2011. [CrossRef] [Google Scholar] [Publisher Link]

[10] Lili Dong, and Silu You, "Adaptive Back-Stepping Control of Active Magnetic Bearings," *2013 10th IEEE International Conference on Control and Automation (ICCA)*, Hangzhou, China, pp. 452-457, 2013. [CrossRef] [Google Scholar] [Publisher Link]

[11] Te-Jen Su et al., "Active Magnetic Bearing System Using PID-surface Sliding Mode Control," *2016 3rd International Conference on Computing Measurement Control and Sensor Network (CMCSN)*, Matsue, Japan, pp. 5-8, 2017. [CrossRef] [Google Scholar] [Publisher Link]

[12] Jason Sheng Hong Tsai et al., "Robust Observer-Based Optimal Linear Quadratic Tracker for Five-Degree-of-Freedom Sampled-Data Active Magnetic Bearing System," *International Journal of Systems Science*, vol. 49, no. 6, pp. 1273-1299, 2018. [CrossRef] [Google Scholar] [Publisher Link]

[13] Bongsob Song, and J. Karl Hedrick, *Dynamic Surface Control of Uncertain Nonlinear Systems*, Springer, 2011. [CrossRef] [Google Scholar] [Publisher Link]

[14] Donald W. Novotny, and Thomas A. Lipo, *Vector Control and Dynamics of {AC} Drives*, Oxford University Press, 1996. [CrossRef] [Google Scholar] [Publisher Link]

[15] Li Feng et al., "Speed Regulation for PMSM Drives Based on a Novel Sliding Mode Controller," *IEEE Access*, vol. 8, pp. 63577-63584, 2020. [CrossRef] [Google Scholar] [Publisher Link]

[16] Trong Duy Nguyen et al., "Modeling and Position-Sensorless Control of a Dual-Airgap Axial Flux Permanent Magnet Machine for Flywheel Energy Storage Systems" *Journal of Power Electronics*, vol. 12, no. 5, pp. 758-768, 2012. [CrossRef] [Google Scholar] [Publisher Link]

[17] Trong Duy Nguyen et al., "A Novel Axial Flux Permanent-Magnet Machine for Flywheel Energy Storage System: Design and Analysis" *IEEE Transactions on Industrial Electronics*, vol. 58, no. 9, pp. 3784-3794, 2011. [CrossRef] [Google Scholar] [Publisher Link]

[18] Trong Duy Nguyen et al., "Modeling and Sensorless Direct Torque and Flux Control of a Dual-Airgap Axial Flux Permanentmagnet Machine with Field-Weakening Operation" *IEEE/ASME Transactions on Mechatronics*, vol. 19, no. 2, pp. 412-422, 2014. [CrossRef] [Google Scholar] [Publisher Link]

[19] Jianfei Zhao, Minqi Hua, and Tingzhang Liu, "Research on a Sliding Mode Vector Control System Based on Collaborative Optimization of an Axial Flux Permanent Magnet Synchronous Motor for an Electric Vehicle," *Energies*, vol. 11, no. 11, pp. 1-16, 2018. [CrossRef] [Google Scholar] [Publisher Link]

[20] Quang Dich Nguyen, and Satoshi Ueno, "Axial Position and Speed Vector Control of the Inset Permanent Magnet Axial Gap Type Self Bearing Motor," *2009 IEEE/ASME International Conference on Advanced Intelligent Mechatronics*, Singapore, pp. 130-135, 2009. [CrossRef] [Google Scholar] [Publisher Link]

[21] Ji-Ye Han, and Shu-Kang Cheng, "Analysis the Electromagnetic Torque and Magnetic Field of the Axial and Radial Air Gap Hybrid Magnet Circuit Multi-Coupling Motor" *2008 International Conference on Electrical Machines and Systems*, Wuhan, China, pp. 3536-3538, 2008. [CrossRef] [Google Scholar] [Publisher Link]

[22] E.H. El Yaagoubi, A. El Assoudi, and H. Hammouri, "High Gain Observe: Attenuation of the Peak Phenomena," *Proceedings of the 2004 American Control Conference*, Boston, MA, USA, vol. 5, pp. 4393-4397, 2004. [CrossRef] [Google Scholar] [Publisher Link]

[23] Daniele Astolfi, and Lorenzo Marconi, "A High-Gain Nonlinear Observe with Limited Gain Power," *IEEE Transactions on Automatic Control*, vol. 60, no. 11, pp. 3059-3064, 2015. [CrossRef] [Google Scholar] [Publisher Link]

[24] Alexis A. Ball, and Hassan K. Khalil, "High-Gain-Observer Tracking Performance in the Presence of Measurement Noise," *2009 American Control Conference*, St. Louis, MO, USA, pp. 4626-4627, 2009. [CrossRef] [Google Scholar] [Publisher Link]

[25] Daehee Won et al., "High-Gain Disturbance Observe-Based Backstepping Control with Output Tracking Error Constraint for Electro-Hydraulic Systems," *IEEE Transactions on Control Systems Technology*, vol. 23, no. 2, pp. 787-795, 2015. [CrossRef] [Google Scholar] [Publisher Link]